

Line-ratio determination of atomic oxygen and $N_2(A^3\Sigma_u^+)$ metastable absolute densities in an RF nitrogen late afterglow

This article has been downloaded from IOPscience. Please scroll down to see the full text article.

2013 Plasma Sources Sci. Technol. 22 035009

(<http://iopscience.iop.org/0963-0252/22/3/035009>)

View [the table of contents for this issue](#), or go to the [journal homepage](#) for more

Download details:

IP Address: 193.136.137.12

The article was downloaded on 04/06/2013 at 10:25

Please note that [terms and conditions apply](#).

Line-ratio determination of atomic oxygen and $N_2(A^3\Sigma_u^+)$ metastable absolute densities in an RF nitrogen late afterglow

André Ricard¹, Soo-ghee Oh² and Vasco Guerra³

¹ Université de Toulouse, UPS, INPT, LAPLACE, 118 route de Narbonne, F-31062 Toulouse, France

² Division of Energy Systems Research, Ajou University, Suwon 443-749, Republic of Korea

³ Instituto de Plasmas e Fusão Nuclear, Instituto Superior Técnico, Universidade Técnica de Lisboa, 1049-001 Lisboa, Portugal

E-mail: vguerra@ist.utl.pt

Received 19 February 2013, in final form 12 April 2013

Published 20 May 2013

Online at stacks.iop.org/PSST/22/035009

Abstract

Optical emission spectroscopy line-ratio methods are developed in order to estimate the absolute densities of nitrogen and oxygen atoms and metastable $N_2(A)$ molecules in the nitrogen late afterglow of an RF discharge, operating at $p = 8$ Torr, $Q = 1$ slm and $P = 100$ W, in what constitutes an extension of the typical domain of application of these methods. $[N]$ is obtained from the first positive (1^+) emission with calibration by NO titration, $[O]$ from the ratio of the NO_β to 1^+ bands, and $[N_2(A)]$ from the ratios of (i) the NO_γ and NO_β bands, (ii) the second positive (2^+) and NO_β bands and (iii) the 1^+ and 2^+ bands. In addition to the determination of the N, O and $N_2(A)$ absolute densities, the present investigation gives an indication on the order of magnitude of the rate coefficient of the very important reaction $N_2(X, v \geq 13) + O \rightarrow NO + N$ at room temperature.

(Some figures may appear in colour only in the online journal)

1. Introduction

Gas discharges in pure nitrogen and in nitrogen-containing mixtures and their afterglows are interesting in very diversified fields, e.g. surface modification of materials [1–4], atmospheric plasma chemistry and investigation of the NO_x and O_3 formation and destruction mechanisms [5–9], or plasma sterilization [10–14]. Nitrogen's first electronically excited state, the metastable triplet $N_2(A^3\Sigma_u^+)$, has an energy threshold of about 6.2 eV and a lifetime ~ 2 s. Therefore, it is an important energy carrier and plays a relevant role in nitrogen discharges and afterglows, being involved in mechanisms as significant as ionization, dissociation, plasma chemistry and gas heating [15–21].

Optical emission spectroscopy is a very convenient plasma diagnostic, since it is relatively simple to perform and does not require very expensive equipment. Its use in the characterization of nitrogen plasmas is so vast that any references given would be merely indicative. The development of line-ratio or 'actinometric' methods, in particular, is spreading quickly [22–32]. They allow the diagnostics of various different quantities, such as the electron field, electron

density, electron temperature, electron energy distribution function and concentration of different species. Most of these diagnostics are used for active discharge conditions, where electron-impact excitation, dissociation and ionization have a central role. In this case, one may find conditions where the interpretation of the results is quite straightforward, for instance, if one species is predominantly created by direct electron impact and lost by radiative decay. However, the advent of more and more complete kinetic models has allowed one to refine the method and to address situations of growing complexity. A recent review of the evolution of line-ratio methods has been made by Zhu and Pu [31]. Clearly, the measurements remain relatively simple even in the more complex cases, although the interpretation becomes difficult and has to rely more and more on the accuracy of the underlying kinetic models.

The existence of rather complete and well-validated nitrogen kinetic models makes it possible to attempt the extension of line-ratio methods to study other conditions, already quite different from those for which they were initially developed. The purpose of this work is precisely to take a

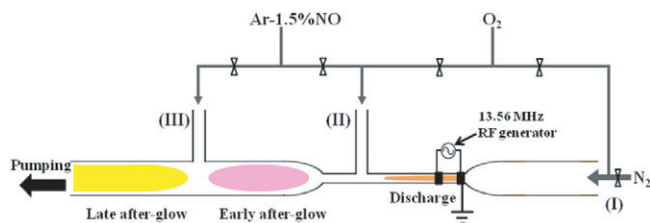


Figure 1. A capacitive RF discharge is generated in a 6 mm i.d. and 30 cm long quartz tube. The flowing afterglow develops downstream in a tube of i.d. equal to 21 mm. An Ar–1.5%NO mixture can be injected after the discharge end (II) or after the early afterglow (III).

firm step in this direction, by investigating the nitrogen late afterglow, where electron processes are no longer present, and to attempt the estimation of metastable $N_2(A)$ molecules, a species that remains hard to measure in relatively simple experiments.

Our method requires the determination of the atomic nitrogen concentration and that of atomic oxygen impurities. The former is obtained from the intensity of the first positive (1^+) emission at 580 nm with calibration by NO titration, while the latter is acquired from the ratio of NO_β to 1^+ bands. $N_2(A)$ is calculated using three independent line-ratio schemes, one involving the NO_γ and NO_β bands, a second one from the second positive (2^+) and NO_β bands, and a third one from the 1^+ and 2^+ bands. It turns out that $N_2(A)$ density derived by the first variant is inversely proportional to the $N_2(X, v) + O \rightarrow NO + O$ reaction rate, subject to large uncertainties up to now. However, this apparent drawback can be turned into an advantage, as the present research can contribute to establish a value for this rate coefficient at room temperature.

The system under analysis is the late afterglow of an RF nitrogen discharge in a quartz tube of inner diameter 6 mm, operating at pressure $p = 8$ Torr, gas flow $Q = 1$ slm and power $P = 100$ W. The afterglow develops in a quartz tube with inner diameter 21 mm. The experiments were conducted using industrial nitrogen (1% impurity) and compared with pure nitrogen gas (10 ppm impurity) as far as [N] and [O] are concerned. Other results for the pink and late afterglow in pure nitrogen and in N_2 – O_2 mixtures have been obtained in [33] for the same conditions.

The structure of the paper is as follows. In the next section we give a very brief description of the experimental setup. The results are presented in section 3, consisting of five subsections. The first is devoted to the determination of the nitrogen atomic concentration in the late afterglow; the second to the estimation of the oxygen atomic density; the third to the calculation of the $N_2(A)$ density using the I_γ/I_β ratio; the fourth to the evaluation of the $N_2(A)$ concentration from the I_{2^+}/I_β ratio; the final one to the determination of the $N_2(A)$ concentration from the I_{1^+}/I_{2^+} ratio. Finally, the main results are summarized in section 4.

2. Experiment

The experimental setup has been previously described in [33] and is reproduced in figure 1. Basically, two quartz tubes of

inner diameter (i.d.) 21 mm are connected to a 6 mm i.d. tube, 30 cm long. The RF plasma is produced in the latter tube, using two rings separated by 2 cm. As depicted in figure 1, the RF discharge corresponds to the most upstream position. Moving downstream from this position three regions can be identified, namely, discharge, early afterglow and late afterglow.

The early or pink afterglow is characterized by a strong emission of the nitrogen first negative system. In this region vibrationally excited $N_2(X^1\Sigma_g^+, v)$ molecules play a significant role in the kinetics [34–36]. The late afterglow is dominated by N-atom three-body recombination, with subsequent emission from the nitrogen first positive system [37–40]. It corresponds to afterglow times ~ 50 ms.

Herein we focus on the late afterglow, where the measurements were performed. For the conditions studied, the most intense emissions were observed for a N_2 flow rate $Q = 1$ slm, pressure $p = 8$ Torr, and incident RF power at 13.56 MHz of 100 W. We carried out experiments using both a pure nitrogen gas (10 ppm impurity) and industrial nitrogen (1% impurity). The former gas is not used in the determination of $N_2(A)$, as not all the emission bands required are visible.

Optical emission spectroscopy measurements were carried out with a Munera 500 optical spectrometer with 500 nm focal length and slits of 0.5 mm and a photomultiplier tube Hamamatsu R928. The nitrogen atomic concentration in the late afterglow was determined by NO titration [33, 37], with an Ar–1.5%NO gas mixture introduced downstream before the late afterglow, position (III) in figure 1. In addition, we have measured the emissions from the first and second positive systems of nitrogen, and from the NO_β and NO_γ bands, corresponding, respectively, to the transitions $N_2(B \rightarrow A)$, $N_2(C \rightarrow B)$, $NO(B \rightarrow X)$ and $NO(A \rightarrow X)$. Further details on the experimental setup can be found in [33].

3. Results and discussion

In this section we present three variants of a line-ratio method allowing the estimation of the $N_2(A)$ metastable density in the late afterglow. The procedure requires a previous estimation of the nitrogen and oxygen atomic concentrations. They can be obtained as well by optical emission spectroscopy, as detailed in sections 3.1 and 3.2. The evaluation of $[N_2(A)]$ is subsequently made in sections 3.3–3.5.

Before proceeding to these estimations, let us just recall that the measured relative intensity $I^m(\lambda_{ij})$ of a band at a certain wavelength λ_{ij} , resulting from the emission of a radiative state R_i^* decaying to a state j , is given by

$$I^m(\lambda_{ij}) = c(\lambda_{ij}) \frac{hc}{\lambda_{ij}} A_{ij} [R_i^*]. \quad (1)$$

Here, $c(\lambda_{ij})$ is the spectral response of the spectrometer at the wavelength λ_{ij} corresponding to the $i \rightarrow j$ transition, h is Planck's constant, c is the value of the speed of light, A_{ij} is the Einstein coefficient for the transition, and $[R_i^*]$ is the density of the emitting radiative state.

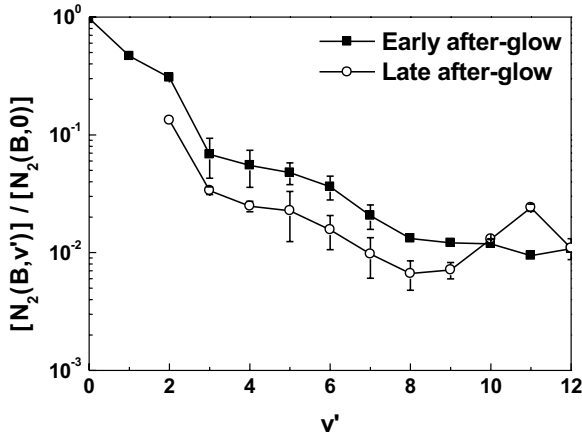
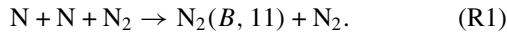


Figure 2. Vibrational distribution function of the $N_2(B^3\Pi_g)$ state in the nitrogen early and late afterglows.

3.1. N-atom density

Figure 2 shows the relative vibrational distribution of the $N_2(B)$ state, $[N_2(B, v')]/[N_2(B, v = 0)]$ both in the early and in the late afterglows. Inspection of the figure reveals a modification in the dominant formation mechanisms of the $N_2(B^3\Pi_g)$ state. As is well known, the three-body recombination process predominantly populates the $N_2(B)$ state in the $v = 11$ level [37–39],

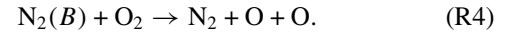
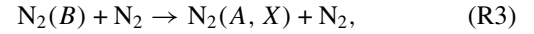
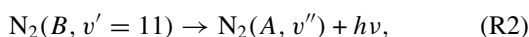


The characteristic peak of the vibrational distribution function at $v = 11$ is thus a signature of reaction (R1). It is observed only in the late afterglow. Therefore, we can conclude that the $N_2(B)$ state is primarily formed by reaction (R1) in this region. However, the overpopulation of level $v = 11$ is not visible in the early afterglow, where $N_2(B)$ is significantly populated in collisions involving $N_2(A)$ metastables and ground-state vibrationally excited molecules $N_2(X, v)$ [34–36]. These states are subsequently quenched and are no longer available in the late afterglow. Such a qualitative interpretation was confirmed by preliminary modeling calculations for the conditions under investigation [41]. A refinement of the model and the detailed analysis of the simulation results will be performed in a future publication.

In order to estimate the nitrogen atomic density in the late afterglow, the expressive emission of the 11-7 band of the first positive system at 580 nm was measured, $N_2(B, v' = 11) \rightarrow N_2(A, v'' = 7) + h\nu(580 \text{ nm})$. This emission ensues the formation of $N_2(B)$ in (R1). According to (1), the $N_2(580 \text{ nm})$ band intensity is given by

$$I^m(580) = c(580) \frac{hc}{580 \text{ nm}} A_{580} [N_2(B, 11)]. \quad (2)$$

We assume that a pseudo-stationary state is achieved for the concentration $[N_2(B, 11)]$ in the late afterglow, resulting from a near equilibrium between its formation by reaction (R1) and its total destruction by radiative decay and quenching. *A priori*, possible $N_2(B, v = 11)$ loss terms are



As we are accounting for the losses of $N_2(B, v = 11)$, reaction (R2) must include all possible v'' levels. The relevant rate coefficients are $k_1 \simeq 4.4 \times 10^{-34} \text{ cm}^6 \text{ s}^{-1}$ [34], $\nu_2 \simeq 2 \times 10^5 \text{ s}^{-1}$ [42, 43], $k_3 \simeq 3 \times 10^{-11} \text{ cm}^3 \text{ s}^{-1}$ [34] and $k_4 \simeq 3 \times 10^{-10} \text{ cm}^3 \text{ s}^{-1}$ [44]. At $p = 8 \text{ Torr}$ and with an O_2 percentage below 1%, it is readily concluded that the dominant loss term is quenching with N_2 , (R3).

From the creation–loss balance, and taking into account the evaluations above, we have

$$[N_2(B, 11)] \simeq \frac{k_1 [N]^2 [N_2]}{k_3 [N_2]} = \frac{k_1}{k_3} [N]^2. \quad (3)$$

The measured intensity $I^m(580 \text{ nm})$ in the late afterglow can then be related to the N-atom density using (2),

$$a_{N+N} I^m(580) \simeq k c(580) A_{580} \frac{k_1}{k_3} [N]^2. \quad (4)$$

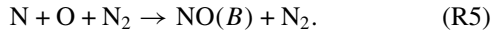
In this expression, a_{N+N} is the fractional contribution of reaction (R1) to the total production of $N_2(B, v = 11)$ molecules, and k is a calibration factor to convert the relative $I^m(580)$ intensity into absolute values. The value of k is established by NO titration in the 2.1 i.d. tube, from the introduction of an Ar–1.5%NO gas mixture downstream before the late afterglow, position (III) in figure 1. Notice that it is only necessary to establish the calibration factor for one particular condition, as from that moment on it is enough to have the intensity $I^m(580)$ to deduce the absolute value $[N]$ in any other situation. In turn, the factor a_{N+N} is determined as detailed in [33]. In practice it represents a mixing between the mechanisms of pure early and late afterglows, and should be equal to one if $N_2(B)$ is produced only through reaction (R1). We have obtained $a_{N+N} \simeq 0.7$ and $a_{N+N} \simeq 1$, respectively, for the cases of pure and industrial nitrogen. Finally, $A_{580} = 7.8 \times 10^4 \text{ s}^{-1}$ [42, 43].

Collecting all the information, the final result is an estimate for the nitrogen atomic concentration in the late afterglow, $[N]$, at $Q = 1 \text{ slm}$, $p = 8 \text{ Torr}$ and $P = 100 \text{ W}$, of the order of $6.5 \times 10^{14} \text{ cm}^{-3}$ and $1.5 \times 10^{15} \text{ cm}^{-3}$, respectively, for pure and industrial nitrogen. A similar increase has been observed by other authors [45–48] and could be due to a change in the self-consistent electric field in the discharge as a consequence of the destruction of the $N_2(A, a')$ states by oxygen [44, 49]. Since these metastable states are involved in stepwise and associative/Penning ionization, direct ionization must compensate for the loss of these ionization channels. As such, the reduced electric field sustaining the discharge must increase. A modification in the N-atom surface recombination probability with small amounts of oxygen has also been suggested as a possible cause contributing to the increase in $[N]$ with oxygen addition [50].

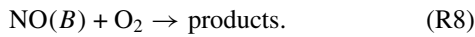
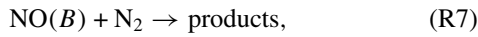
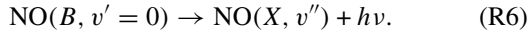
3.2. O-atom density

The presence of the NO_β bands in the late afterglow makes it possible to estimate the oxygen atomic density in this region,

because the emitting $\text{NO}(B)$ state is formed in the three-body reaction involving O atoms



We have followed the NO_β emission at 320 nm, corresponding to the $\text{NO}(B, v' = 0)$ to $\text{NO}(X, v'' = 8)$ transition, $\text{NO}(B, v' = 0) \rightarrow \text{NO}(X, v'' = 8) + h\nu(320 \text{ nm})$. Possible $\text{NO}(B)$ destruction mechanisms are



In the last two reactions, part of $\text{NO}(B)$ may dissociate or be deactivated to excited $\text{NO}(A)$ or to $\text{NO}(X)$ [51]. The rate coefficients of processes (R5)–(R8) are approximately $k_5 \simeq 3.1 \times 10^{-34} \text{ cm}^6 \text{ s}^{-1}$ [12], $\nu_6 \simeq 4.7 \times 10^5 \text{ s}^{-1}$ [42, 43], $k_7 \simeq 6.1 \times 10^{-13} \text{ cm}^3 \text{ s}^{-1}$ [52] and $k_8 \simeq 1.5 \times 10^{-11} \text{ cm}^3 \text{ s}^{-1}$ [52]. As the percentage of O_2 is always below 1%, the quenching of $\text{NO}(B)$ by O_2 , (R8), can be neglected as compared with the one by N_2 , (R7).

The pseudo-stationary concentration of $[\text{NO}(B)]$ in the late afterglow can be calculated, in consonance with the approximations already detailed, from

$$[\text{NO}(B)] \simeq \frac{k_5[\text{N}][\text{O}][\text{N}_2]}{\nu_6 + k_7[\text{N}_2]}. \quad (5)$$

Substituting $[\text{NO}(B)]$ using (1)

$$I^m(320) \simeq c(320) \frac{hc}{320 \text{ nm}} A_{320} \frac{k_5[\text{N}][\text{O}][\text{N}_2]}{\nu_6 + k_7[\text{N}_2]}, \quad (6)$$

where $A_{320} \simeq 8.3 \times 10^4 \text{ s}^{-1}$ [42] is the Einstein coefficient of the $\text{NO}_\beta(0-8)$ transition. Finally, taking the ratio of the measured intensities of the 580 nm and the 320 nm lines, we obtain

$$a_{\text{N+N}} \frac{I^m(580)}{I^m(320)} \simeq \frac{c(580) 580 A_{580} (k_1/k_3)[\text{N}]}{c(320) 320 A_{320} k_5[\text{O}][\text{N}_2]} (\nu_6 + [\text{N}_2]k_7). \quad (7)$$

This equation provides the estimation of the oxygen atomic concentration if $[\text{N}]$ and the spectral responses $c(\lambda)$ are known. The latter were measured with a calibrated W ribbon. For our spectrometer, we found $c(320) = 1 \text{ a.u.}$ and $c(580) = 0.13 \text{ a.u.}$

We have now all the quantities required to estimate the atomic concentration $[\text{O}]$ from equation (7). Using the previously determined N-atom concentration of $6.5 \times 10^{14} \text{ cm}^{-3}$ and $1.5 \times 10^{15} \text{ cm}^{-3}$ we obtain $[\text{O}] \simeq 9 \times 10^{12} \text{ cm}^{-3}$ and $[\text{O}] \simeq 7 \times 10^{14} \text{ cm}^{-3}$, respectively, for the pure and industrial nitrogen gases, i.e. impurity ratios $[\text{O}]/[\text{N}_2]$ of about 35 ppm and 0.3%, respectively. Note that the value of 35 ppm deduced for the pure nitrogen gas implies that the observed oxygen is not coming exclusively from the feed gas, but also from micro-leaks in the reactor.

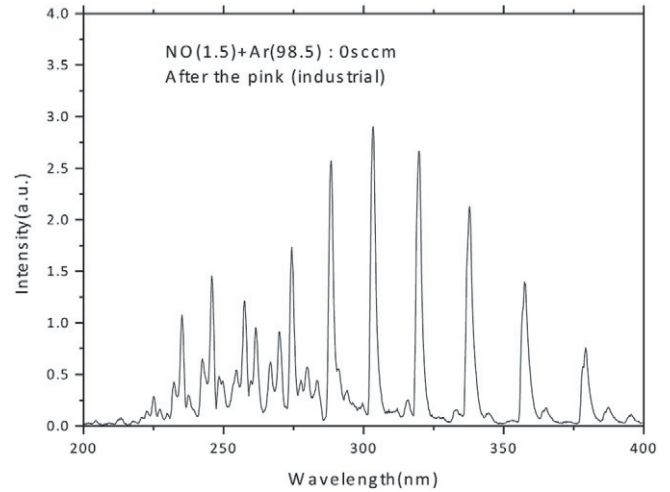


Figure 3. Emission of the NO_γ and NO_β bands in the late afterglow; industrial N_2 (99% purity), 1 slm, 8 Torr and 100 W.

3.3. $\text{N}_2(A)$ density from the I_γ/I_β ratio

As the densities $[\text{N}]$ and $[\text{O}]$ have already been obtained, it is now possible to use optical emission spectroscopy to estimate the density of $\text{N}_2(A)$ metastables in the late afterglow and for the industrial nitrogen case, where all the NO bands are clearly visible. We do so using three different line ratios. The first one is the ratio of the NO_γ emission at 259 nm, corresponding to the transition $\text{NO}(A, v' = 0) \rightarrow \text{NO}(X, v'' = 3) + h\nu(259 \text{ nm})$, to the NO_β emission at 262 nm, due to the $\text{NO}(B, v' = 0) \rightarrow \text{NO}(X, v'' = 4) + h\nu(262 \text{ nm})$ transition. The second one is the ratio of the nitrogen 2^+ system at 316 nm, $\text{N}_2(C, v' = 1) \rightarrow \text{N}_2(B, v'' = 0) + h\nu(316 \text{ nm})$ to the NO_β band at 320 nm already used in the determination of the oxygen atomic density. The choice of transitions with neighboring wavelengths for the line ratios has the small advantages of narrowing the wavelength range to scan and making it possible to neglect any variation of the spectral response $c(\lambda)$ (see expression (1)). We will additionally determine $[\text{N}_2(A)]$ from the ratio of the 1^+ band at 580 nm to the 2^+ one at 316 nm. For now we discuss the I_γ/I_β procedure, whereas the remaining ones are presented in the subsequent sections.

The emission spectrum showing the NO_γ ($\lambda < 260 \text{ nm}$) and NO_β ($\lambda > 260 \text{ nm}$) bands in the late afterglow (after position III in figure 1) is given in figure 3, for the case of industrial N_2 (99% purity) and without external Ar–1.5%NO addition. Therefore, the emissions of the NO_γ and NO_β bands observed in this figure are only a result of the O and NO impurities in the industrial N_2 gas.

The variation of the intensities of the bands at 259 and 262 nm in the late afterglow as a function of the Ar–1.5%NO introduced in the late afterglow is represented in figure 4, for the industrial nitrogen gas. As can be seen, the intensities $I^m(259)$ and $I^m(262)$ are nearly the same up to 350 sccm of Ar–1.5%NO, where the extinction point is observed. The latter condition is at the basis of the NO titration method and allows the determination of the N-atom density [33, 37].

The intensity of the NO_β band $I^m(262)$ is given similarly by equation (6). In turn, the observed intensity of the NO_γ

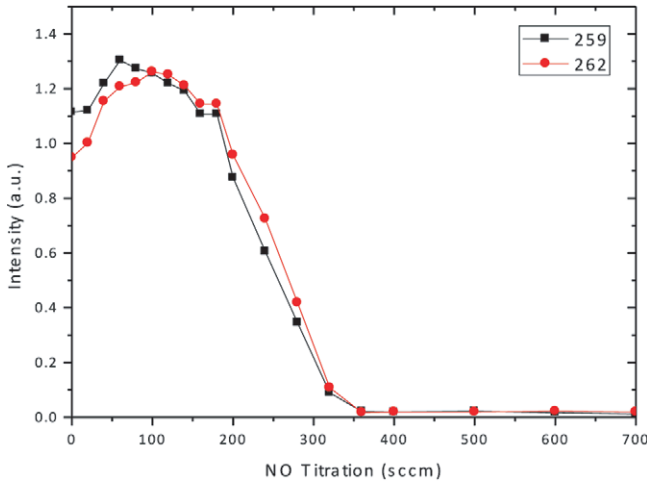
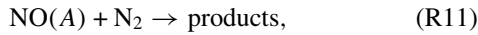
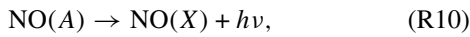
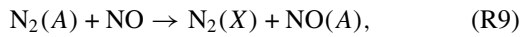


Figure 4. Intensities of the NO_γ (259 nm) and NO_β (262 nm) bands in the late afterglow; industrial N_2 (99% purity), 1 slm, 8 Torr and 100 W.

band $I^m(259)$ can be explained by the three reactions



where NO in reaction (R9) is coming essentially from the NO added into the late afterglow as part of the titration procedure. The corresponding rate coefficients are $k_9 = 6.6 \times 10^{-11} \text{ cm}^3 \text{ s}^{-1}$ [44], $\nu_{10} = 5 \times 10^6 \text{ s}^{-1}$ [52] and $k_{11} = 10^{-13} \text{ cm}^3 \text{ s}^{-1}$ [52]. Hence, we can write

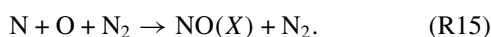
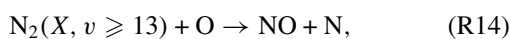
$$\begin{aligned} I^m(259) &= c(259) \frac{hc}{259 \text{ nm}} A_{259} [\text{NO}(\text{A})] \\ &\simeq c(259) \frac{hc}{259 \text{ nm}} A_{259} \frac{k_9 [\text{N}_2(\text{A})] [\text{NO}]}{\nu_{10} + k_{11} [\text{N}_2]}. \end{aligned} \quad (8)$$

The ratio of the intensities of the NO_γ and NO_β bands, given by expressions (8) and (6) (with 320 nm replaced by 262 nm), can be written as

$$\frac{I^m(259)}{I^m(262)} \simeq \frac{A_{259} k_9 [\text{N}_2(\text{A})] [\text{NO}]}{A_{262} k_5 [\text{N}] [\text{O}] [\text{N}_2]} \frac{\nu_6 + k_7 [\text{N}_2]}{\nu_{10} + k_{11} [\text{N}_2]}, \quad (9)$$

where we have neglected the variations in the spectral responses $c(\lambda)$ between 259 and 262 nm, and have approximated $262/259 \simeq 1$, $A_{259} = 7.7 \times 10^5 \text{ s}^{-1}$ and $A_{262} = 2.4 \times 10^4 \text{ s}^{-1}$ [42, 43].

In order to use equation (9), we still need to estimate the ratio $[\text{NO}]/[\text{O}]$. The atomic oxygen concentration determined in section 3.2 cannot be used here, as the introduction of NO will change its value. A simplified kinetics of atomic oxygen in the late afterglow can be described by



The pseudo-stationary density $[\text{O}]$ can then be obtained from

$$\begin{aligned} k_{12} [\text{N}] [\text{NO}] &\simeq (k_{15} [\text{N}] [\text{N}_2] + k_{13} [\text{N}_2(\text{A})] \\ &+ k_{14} [\text{N}_2(\text{X}, v \geq 13)]) [\text{O}]. \end{aligned} \quad (10)$$

Therefore, the required $[\text{NO}]/[\text{O}]$ ratio is given by

$$\frac{[\text{NO}]}{[\text{O}]} \simeq \frac{k_{15} [\text{N}] [\text{N}_2] + k_{13} [\text{N}_2(\text{A})] + k_{14} [\text{N}_2(\text{X}, v \geq 13)]}{k_{12} [\text{N}]}. \quad (11)$$

The rate coefficients of processes (R12) and (R13) are $k_{12} = 1.8 \times 10^{-11}$ [44] and $k_{13} = 7 \times 10^{-12} \text{ cm}^3 \text{ s}^{-1}$. Regarding reaction (R14), there are large uncertainties in the value of its coefficient. As the reaction is exothermic for $v \geq 13$, it is expected that the rate coefficient strongly increases for $v \lesssim 13$, exhibiting a smoother rise for $v > 13$. In previous modeling studies, simple step functions in the range 10^{-13} – $10^{-11} \text{ cm}^3 \text{ s}^{-1}$ have been used [44, 49]. Bose and Candler present a quasiclassical trajectory (QCT) calculation of this rate [53], but they only calculate data for high temperatures. For instance, for rotational equilibrium with a rotational temperature equal to the gas temperature, $T = 7000 \text{ K}$, they report values of $8 \times 10^{-12} \text{ cm}^3 \text{ s}^{-1}$, $2.6 \times 10^{-11} \text{ cm}^3 \text{ s}^{-1}$ and $5 \times 10^{-11} \text{ cm}^3 \text{ s}^{-1}$, respectively, for $v = 10, 15$ and 20 . However, extrapolation of these values to lower temperatures is far from trivial. In order to try to address this question, calculations of these rate coefficients using the forced harmonic oscillator model [54–57] will be performed in the future. However, theoretical calculations by Macheret and co-workers [58, 59] foresee that the actual reaction paths are different at low temperatures ($T < 2000 \text{ K}$) and high temperatures ($T > 2000 \text{ K}$). In the former case, an electronically non-adiabatic curve-crossing mechanism is favored, involving multiquantum vibrational transitions at the intersection of the electronic terms of the $\text{N}_2\text{--O}$ system and the formation of the intermediate long-lived complex $\text{N}_2\text{O}(\text{X}^1\Sigma^+)$. The calculated probabilities for the non-adiabatic reaction for $T \leq 1000 \text{ K}$ are in the range 10^{-2} – 10^{-3} , translating into a pre-exponential factor of 10^{-13} – $10^{-12} \text{ cm}^3 \text{ s}^{-1}$ for a vibrational temperature of the lower v -levels $T_v \simeq 3000 \text{ K}$ [59]. Note that the electronically adiabatic channel would have a rate coefficient at room temperature orders of magnitude lower [59]. Due to the lack of data, for the moment we will consider $k_{14} = 10^{-13}$ – $10^{-11} \text{ cm}^3 \text{ s}^{-1}$. Finally, the rate coefficient of reaction (R15) is $k_{15} = 10^{-32} \text{ cm}^6 \text{ s}^{-1}$, 32 times higher than the partial rate for $\text{NO}(\text{B})$ production in process (R5).

It is relatively easy to show that, for the present conditions, the dominant loss frequency in equation (11) is due to reaction (R14). Using $[\text{N}] \simeq 1.5 \times 10^{15} \text{ cm}^{-3}$, as concluded in section 3.1, the loss frequency of reaction (R15) is $k_{15} [\text{N}] [\text{N}_2] \sim 4 \text{ s}^{-1}$. Next, for relative $\text{N}_2(\text{A})$ densities below 5×10^{-5} , as is typical for nitrogen afterglows in this range of pressure [36], the loss term in process (R13) is $k_{13} [\text{N}_2(\text{A})] < 90 \text{ s}^{-1}$. Finally, to estimate the atomic oxygen losses in the NO formation mechanism (R14) we assume that $[\text{N}_2(\text{X}, v \geq 13)] \sim 5 \times 10^{-3} [\text{N}_2]$ [60], so that $k_{14} [\text{N}_2(\text{X}, v \geq 13)] \sim 1.2 \times (10^2\text{--}10^4) \text{ s}^{-1}$, depending on the value of k_{14} . In passing, let us note that the atomic oxygen losses at the wall occur at a frequency of about 1 s^{-1} for a wall recombination

probability γ_O of the order of 10^{-4} [61, 62], or 10 times higher for $\gamma_O \sim 10^{-3}$ [63, 64], so they can be neglected as well in the present evaluation.

In this way, equation (11) can be approximated by

$$\frac{[\text{NO}]}{[\text{O}]} \simeq \frac{k_{14}[\text{N}_2(x, v \geq 13)]}{k_{12}[\text{N}]} \quad (12)$$

Substituting in (9),

$$\frac{I^m(259)}{I^m(262)} \simeq \frac{A_{259} k_9 [\text{N}_2(A)] \nu_6 + k_7 [\text{N}_2]}{A_{262} k_5 [\text{N}] [\text{N}_2] \nu_{10} + k_{11} [\text{N}_2]} \frac{k_{14} [\text{N}_2(x, v \geq 13)]}{k_{12} [\text{N}]} \quad (13)$$

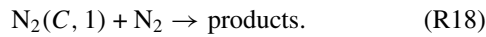
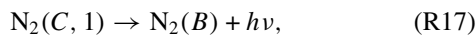
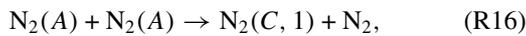
Apart from the uncertainties surrounding the coefficient k_{14} , the only unknown in this expression is the concentration $[\text{N}_2(A)]$. Thus, the density of this metastable state in the afterglow can be estimated by the line ratio $I^m(259)/I^m(262)$.

From figure 4, for the industrial N_2 gas $I^m(259)/I^m(262) = 1.2$ when the introduced NO in the late afterglow approaches zero. Substituting all the values in equation (13), the final result for the $\text{N}_2(A)$ concentration in the late afterglow $[\text{N}_2(A)] \simeq 1.1 \times 10^9 - 1.1 \times 10^{11} \text{ cm}^{-3}$, as k_{14} decreases from 10^{-11} to $10^{-13} \text{ cm}^3 \text{ s}^{-1}$.

It is worth noting that with the pure nitrogen gas a mixed late and pink afterglow ($a_{\text{N+N}} = 0.7$) was observed. That being so, in that case $\text{N}_2(A)$ metastables may be partially formed in reactions involving vibrationally excited molecules $\text{N}_2(X, v)$ as in the pink afterglow [36, 60]. In contrast, the nearly identical variations of the NO_γ and NO_β bands detected in figure 3 suggest that for industrial nitrogen $\text{N}_2(A)$ molecules are following the nitrogen atoms. This means they are mainly produced as a result of three-body N recombination, either directly or via a formation of the $\text{N}_2(B)$ state and subsequent quenching to $\text{N}_2(A)$.

3.4. $\text{N}_2(A)$ density from the I_{2^+}/I_β ratio

Another possibility to estimate the $\text{N}_2(A)$ metastable density in the late afterglow is given by the line ratio of the 2^+ system at 316 nm, $\text{N}_2(C, 1-B, 0)$ with the $\text{NO}_\beta(0-8)$ band at 320 nm. The dominant reactions responsible for the 2^+ emission in the late afterglow are



The rate coefficient of reaction (R16) is $k_{16} = 4.1 \times 10^{-11} \text{ cm}^3 \text{ s}^{-1}$ [65], where it was assumed that most of the $\text{N}_2(A)$ molecules are in the ground vibrational level. The loss rates of $\text{N}_2(C, v' = 1)$ molecules are given by $\nu_{17} = 2.7 \times 10^7 \text{ s}^{-1}$ [42, 43] and $k_{18} = 3 \times 10^{-11} \text{ cm}^3 \text{ s}^{-1}$ [66, 67].

In accordance with mechanisms (R16)–(R18), we can write

$$\begin{aligned} I^m(316) &= c(316) \frac{hc}{316 \text{ nm}} A_{316} [\text{N}_2(C)] \\ &\simeq c(316) \frac{hc}{316 \text{ nm}} A_{316} \frac{k_{16} [\text{N}_2(A)]^2}{\nu_{17} + k_{18} [\text{N}_2]}, \end{aligned} \quad (14)$$

where $A_{316} = 1.3 \times 10^7 \text{ s}^{-1}$ [42, 43]. Using (6) we finally obtain

$$\frac{I^m(320)}{I^m(316)} \simeq \frac{A_{320} k_5 [\text{N}] [\text{O}] [\text{N}_2] \nu_{17} + k_{18} [\text{N}_2]}{A_{316} k_{16} [\text{N}_2(A)]^2 \nu_6 + k_7 [\text{N}_2]}. \quad (15)$$

The concentration of $\text{N}_2(A)$ metastables can be determined from (15). For the industrial nitrogen gas the measured $I^m(320)/I^m(316)$ ratio is 13, from which it follows that $[\text{N}_2(A)] \sim 2.4 \times 10^{11} \text{ cm}^3 \text{ s}^{-1}$.

3.5. $\text{N}_2(A)$ density from the I_{1^+}/I_{2^+} ratio

One last easy estimation of $\text{N}_2(A)$ can still be made, making use of bands already analyzed. As a matter of fact, the ratio of the 1^+ emission at 580 nm, given by (2) and (3), to the 2^+ emission at 316 nm, expressed in (14), is

$$\frac{I^m(580)}{I^m(316)} \simeq \frac{c(580) A_{580} 316}{c(316) A_{316} 580} \frac{k_1 [\text{N}]^2}{k_3 k_{15} [\text{N}_2(A)]^2} (\nu_{16} + k_{17} [\text{N}_2]). \quad (16)$$

The experimental ratio is 2.24, leading to the result $[\text{N}_2(A)] \sim 7.3 \times 10^{10} \text{ cm}^3 \text{ s}^{-1}$.

4. Conclusions

In this work we have shown that optical emission spectroscopy line-ratio methods are extremely powerful and can be extended far beyond their typical domain of application. In particular, we have developed a procedure to obtain the absolute densities of N and O atoms and $\text{N}_2(A)$ metastable molecules in the nitrogen late afterglow. An RF discharge was generated at $p = 8$ Torr, $P = 100$ W, $Q = 1$ slm, in a quartz tube of inner diameter 6 mm, whereas the afterglow developed in a quartz tube of i.d. 21 mm. The experiments were conducted using both pure nitrogen (10 ppm impurity) and industrial nitrogen (1% impurity). However, due to the difficulty in the detection of all the NO bands, the $\text{N}_2(A)$ concentration was derived only for the case of industrial nitrogen.

The nitrogen atomic density in the late afterglow was determined from the emission of the 1^+ nitrogen system $\text{N}_2(11-7)$ at 580 nm, while the oxygen atomic density was derived from the ratio of the $\text{NO}_\beta(0-8)$ band at 320 nm to the 580 nm line. The $\text{N}_2(A)$ metastable concentration was estimated using three different line-ratios, the ratio of the $\text{NO}_\gamma(0-3)$ band at 259 nm to the $\text{NO}_\beta(0-4)$ band at 262 nm, the ratio of the $\text{N}_2 2^+$ band (1-0) at 316 nm to the 320 nm band, and the ratio of the previously used 1^+ 580 nm and 2^+ 316 nm bands. The results are summarized in table 1. Note that the uncertainties indicated in the table refer only to the experimental errors. As such, they do not include the influence of any doubts surrounding the reaction rate coefficients nor of the pseudo-stationary approach inherent in the method.

The three methods to determine the $\text{N}_2(A)$ concentration lead to rather consistent results, pointing to a value of the order of $\sim 10^{11} \text{ cm}^{-3}$. One possible reason for the slightly higher value deduced from the I_γ/I_β and I_{2^+}/I_β ratios could be the contribution of reaction (R8) and/or of the similar reaction involving NO, $\text{NO}(B) + \text{NO} \rightarrow \text{products}$ already competitive

Table 1. Absolute densities in cm^{-3} estimated in the late afterglow: $p = 8$ Torr, $Q = 1$ slm, $P = 100$ W.

Species	Lines	Pure N ₂	Industrial N ₂	Uncertainty
[N]	$I_{1+}(580)$	6×10^{14}	1.5×10^{15}	30%
[O]	$I_{\beta}(320)/I_{1+}(580)$	9×10^{12}	7×10^{14}	50%
[N ₂ (A)]	$I_{\gamma}(259)/I_{\beta}(262)$	—	$1.1 \times (10^9-10^{11})$	70%
[N ₂ (A)]	$I_{2+}(316)/I_{\beta}(320)$	—	2.4×10^{11}	45%
[N ₂ (A)]	$I_{1+}(580)/I_{2+}(316)$	—	7.3×10^{10}	35%

with that of (R7). Note that $k_7 = 6.1 \times 10^{-13} \text{ cm}^3 \text{ s}^{-1}$, $k_8 = 1.5 \times 10^{-11} \text{ cm}^3 \text{ s}^{-1}$, while $k_{\text{NO}} = 2 \times 10^{-10} \text{ cm}^3 \text{ s}^{-1}$ [52]. This would imply a correction in the denominator of expression (15), to be read $v_6 + k_7[\text{N}_2] + k_8[\text{O}_2] + k_{\text{NO}}[\text{NO}]$, with the consequent decrease in the estimated value for $[\text{N}_2(\text{A})]$.

The range of possible values for $[\text{N}_2(\text{A})]$ calculated from the $I_{\gamma}(259)/I_{\beta}(262)$ ratio correspond to the uncertainty in the rate coefficient of the NO formation reaction $\text{N}_2(\text{X}, v \geq 13) + \text{O} \rightarrow \text{NO} + \text{N}$, k_{14} , between 10^{-13} and $10^{-11} \text{ cm}^3 \text{ s}^{-1}$, the lower value of the rate coefficient corresponding to the higher $\text{N}_2(\text{A})$ density. Comparison with the result obtained from the $I_{2+}(316)/I_{\beta}(320)$ ratio suggests a rate coefficient close to $10^{-13} \text{ cm}^3 \text{ s}^{-1}$. However, preliminary model calculations [41] for the conditions and measurements presented in [33] would suggest instead a value of $10^{-11} \text{ cm}^3 \text{ s}^{-1}$ and/or a higher deactivation of vibrationally excited molecules $\text{N}_2(\text{X}, v)$ by O atoms than normally considered [44, 49]. Hence, the present results point toward a value for k_{14} of the order of $10^{-13} \text{ cm}^3 \text{ s}^{-1}$ and a stronger deactivation of intermediate and high $\text{N}_2(\text{X}, v)$ vibrational levels by oxygen atoms than previously proposed. This finding is consistent with the mechanisms and theoretical predictions from [58, 59]. The development of a complete self-consistent model to further investigate and clarify these questions from the comparison of the simulation predictions with the present results and those of Kang *et al* [33] is under way and will be presented in a forthcoming publication.

Acknowledgments

This work was partially supported by the National Research Foundation of Korea (NRF) grant funded by the Korean government (MEST) (No 2012034915). VG was supported by the Portuguese Fundação para a Ciência e Tecnologia (FCT) funds to Instituto de Plasmas e Fusão Nuclear–Laboratório Associado.

References

- [1] Cheng Z, Li C X, Dong H and Bell T 2005 Low temperature plasma nitrocarburising of AISI 316 austenitic stainless steel *Surf. Coat. Technol.* **191** 195–200
- [2] Jaoul C, Belmonte T, Czerwiec T, Ablitzer D, Ricard A and Michel H 2006 Iron nitrocarburising in flowing post-discharge: evolution of the compound layer *Thin Solid Films* **506–507** 163–7
- [3] Wang J, Xiong J, Peng Q, Fana H, Wang Y, Li G and Shen B 2009 Effects of DC plasma nitriding parameters on microstructure and properties of 304L stainless steel *Mater. Charact.* **60** 197–203
- [4] Fernandes F A P, Heck S, Pereira R G, Lombardi-Neto A, Totten G E and Casteletti L C 2010 Wear of plasma nitrided and nitrocarburized AISI 316L austenitic stainless steel *J. Achiev. Mater. Manuf. Eng.* **40** 175–9
- [5] Stefanović I, Bibinov N K, Deryugin A A, Vinogradov I P, Napartovich A P and Wiesemann K 2001 Kinetics of ozone and nitric oxides in dielectric barrier discharges in O_2/NO_x and $\text{N}_2/\text{O}_2/\text{NO}_x$ mixtures *Plasma Sources Sci. Technol.* **10** 406–16
- [6] Baeva M, Gier H, Pott A, Uhlenbusch J, Höschele J and Steinwandel J 2002 Pulsed microwave discharge at atmospheric pressure for NO_x decomposition *Plasma Sources Sci. Technol.* **11** 1–9
- [7] Okubo M, Inoue M, Kuroki T and Yamamoto T T 2005 NO_x reduction after treatment system using nitrogen nonthermal plasma desorption *IEEE Trans. Indust. Appl.* **41** 891–9
- [8] Guaitella O, Hübner M, Welzel S, Marinov D, Röpcke J and Rousseau A 2010 Evidence for surface oxidation on Pyrex of NO into NO_2 by adsorbed O atoms *Plasma Sources Sci. Technol.* **19** 45026
- [9] Welzel S, Guaitella O, Lazzaroni C, Pintassilgo C D, Rousseau A and Röpcke J 2011 NO kinetics in pulsed low-pressure plasmas studied by time-resolved quantum cascade laser absorption spectroscopy *Plasma Sources Sci. Technol.* **20** 015020
- [10] Villegier S, Cousty S, Ricard A and Sixou M 2003 Sterilization of E-coli bacterium in a flowing $\text{N}_2\text{--O}_2$ post-discharge reactor *J. Phys. D: Appl. Phys.* **36** L60–2
- [11] Pintassilgo C D, Kutasi K and Loureiro J 2007 Modelling of a low-pressure $\text{N}_2\text{--O}_2$ discharge and post-discharge reactor for plasma sterilization *Plasma Sources Sci. Technol.* **16** S115–22
- [12] Kutasi K, Saoudi B, Pintassilgo C D, Loureiro J and Moisan M 2008 Modelling the low-pressure $\text{N}_2\text{--O}_2$ plasma afterglow to determine the kinetic mechanisms controlling the UV emission intensity and its spatial distribution for achieving an efficient sterilization process *Plasma Process. Polym.* **5** 840–52
- [13] Singh M K, Ogino A and Nagatsu M 2009 Inactivation factors of spore-forming bacteria using low-pressure microwave plasmas in an N_2 and O_2 gas mixture *New J. Phys.* **11** 115027
- [14] Boudam M K, Saoudi B, Moisan M and Ricard A 2007 Characterization of the flowing afterglows of an $\text{N}_2\text{--O}_2$ reduced-pressure discharge: setting the operating conditions to achieve a dominant late afterglow and correlating the NO_β UV intensity variation with the N and O atom densities *J. Phys. D: Appl. Phys.* **40** 1694–711
- [15] Benedictis S D, Dilecce G and Simek M 1993 Time-resolved LIF spectroscopy on $\text{N}_2(\text{A})$ metastable in a He/ N_2 pulsed rf discharge *Chem. Phys.* **178** 547–60
- [16] Guerra V, Sá P A and Loureiro J 2001 Role played by the $\text{N}_2(\text{A } ^3\Sigma_u^+)$ metastable in stationary N_2 and $\text{N}_2\text{--O}_2$ discharges *J. Phys. D: Appl. Phys.* **34** 1745–55
- [17] Loureiro J, Sá P A and Guerra V 2001 Role of long-lived $\text{N}_2(\text{X } ^1\Sigma_u^+, v)$ molecules and $\text{N}_2(\text{A } ^3\Sigma_u^+)$ and $\text{N}_2(\text{a } ^1\Sigma_u^-)$ states in the light emissions of a N_2 afterglow *J. Phys. D: Appl. Phys.* **34** 1769–78

- [18] Popov N A 2011 Fast gas heating in a nitrogen–oxygen discharge plasma: I. Kinetic mechanism *J. Phys. D: Appl. Phys.* **44** 285201
- [19] Mintousov E I, Pendleton S J, Gerbault F G, Popov N A and Starikovskaia S M 2011 Fast gas heating in nitrogen–oxygen discharge plasma: II. Energy exchange in the afterglow of a volume nanosecond discharge at moderate pressures *J. Phys. D: Appl. Phys.* **44** 285202
- [20] Horikawa Y, Hayashi T and Sasaki K 2012 Lifetime of molecular nitrogen at metastable $A^3\Sigma_u$ state in afterglow of inductively-coupled nitrogen plasma *Japan. J. Appl. Phys.* **51** 126301
- [21] Nemschokmichal S and Meichsner J 2013 $N_2(A^3\Sigma_u^+)$ metastable density in nitrogen barrier discharges: I. LIF diagnostics and absolute calibration by rayleigh scattering *Plasma Sources Sci. Technol.* **22** 015005
- [22] Bibinov N K, Kokh D B, Kolokolov N B, Kostenko V A, Meyer D, Vinogradov I P and Wiesemann K 1998 A comparative study of the electron distribution function in the positive columns in N_2 and N_2/He dc glow discharges by optical spectroscopy and probes *Plasma Sources Sci. Technol.* **7** 298–309
- [23] Kozlov K V, Wagner H E, Brandenburg R and Michel P 2001 Spatio-temporally resolved spectroscopic diagnostics of the barrier discharge in air at atmospheric pressure *J. Phys. D: Appl. Phys.* **34** 3164–76
- [24] Zhu X M and Pu Y K 2005 Determining the electron temperature in inductively coupled nitrogen plasmas by optical emission spectroscopy with molecular kinetic effects *Phys. Plasmas* **12** 103501
- [25] Paris P, Aints M, Valk F, Plank T, Haljaste A, Kozlov K V and Wagner H E 2005 Intensity ratio of spectral bands of nitrogen as a measure of electric field strength in plasmas *J. Phys. D: Appl. Phys.* **38** 3894–9
- [26] Lebedev Yu A and Shakhmatov V A 2006 Diagnostics of a nonequilibrium nitrogen plasma from the emission spectra of the second positive system of N_2 *Plasma Phys. Rep.* **32** 56–71
- [27] Zhu X M, Pu Y D, Guo Z G and Pu Y K 2006 A novel method to determine electron density by optical emission spectroscopy in low-pressure nitrogen plasmas *Phys. Plasmas* **13** 123501
- [28] Britun N, Gaillard M, Ricard A, Kim Y M, Kim K S and Han J G 2007 Determination of the vibrational, rotational and electronic temperatures in N_2 and Ar– N_2 discharges *J. Phys. D: Appl. Phys.* **40** 1022–9
- [29] Zhu X M and Pu Y K 2008 Using OES to determine electron temperature and density in low-pressure nitrogen and argon plasmas *Plasma Sources Sci. Technol.* **17** 024002
- [30] Isola L M, Gómez B J and Guerra V 2010 Determination of the electron temperature and density in the negative glow of a nitrogen pulsed discharge using optical emission spectroscopy *J. Phys. D: Appl. Phys.* **43** 015202
- [31] Zhu X M and Pu Y K 2010 Optical emission spectroscopy in low-temperature plasmas containing argon and nitrogen: determination of the electron temperature and density by the line-ratio method *J. Phys. D: Appl. Phys.* **43** 403001
- [32] Starikovskaia S M, Allegraud K, Guaitella O and Rousseau A 2010 On electric field measurements in surface dielectric barrier discharge *J. Phys. D: Appl. Phys.* **43** 124007
- [33] Kang N, Lee M, Ricard A and Oh S 2012 Effect of controlled O_2 impurities on N_2 afterglows of RF discharges *Curr. Appl. Phys.* **12** 1448–53
- [34] Guerra V and Loureiro J 1997 Electron and heavy particle kinetics in a low pressure nitrogen glow discharge *Plasma Sources Sci. Technol.* **6** 361–72
- [35] Guerra V, Sá P A and Loureiro J 2003 Electron and metastable kinetics in the nitrogen afterglow *Plasma Sources Sci. Technol.* **12** S8–S15
- [36] Guerra V, Sá P A and Loureiro J 2004 Kinetic modeling of low-pressure nitrogen discharges and post-discharges *Eur. Phys. J. Appl. Phys.* **28** 125–52
- [37] Mérel P, Tabbal M, Chaker M, Moisan M and Ricard A 1998 Influence of the field frequency on the nitrogen atom yield in the remote plasma of an N_2 high frequency discharge *Plasma Sources Sci. Technol.* **7** 550–6
- [38] Diamy A M, Hochard L, Legrand J C and Ricard A 1998 Concentrations of active species in the flowing afterglow of a nitrogen microwave plasma *Plasma Chem. Plasma Process.* **18** 447–60
- [39] Levaton J, Amorim J and Franco D 2005 Experimental and calculated $N(^4S)$ temporal density profile in the N_2 flowing post-discharge *J. Phys. D: Appl. Phys.* **38** 2204–10
- [40] Babayan S E, Ding G and Hicks R F 2001 Determination of the nitrogen atom density in the afterglow of nitrogen and helium, nonequilibrium, atmospheric pressure plasma *Plasma Chem. Plasma Process.* **21** 505–21
- [41] Guerra V, Kang N, Lee M, Oh S and Ricard A 2012 Kinetics of the nitrogen pink afterglow in the presence of oxygen impurities *Proc. 21st ESCAMPIG (Europhysics Conf. on the Atomic and Molecular Physics of Ionized Gases) (Viana do Castelo, Portugal)* ed P G C Almeida et al, P1.9.7
- [42] Laux C O and Kruger C H 1992 Arrays of radiative transition probabilities for the N_2 first and second positive, and O_2 Schumann–Runge band systems *J. Quant. Spectrosc. Radiat. Transfer* **48** 9–24
- [43] Lino da Silva M 2005 Instituto Superior Técnico, Gas and plasma radiation database (gprd) <http://cfp.ist.utl.pt/radiation/gprd/index.php>
- [44] Guerra V and Loureiro J 1997 Self-consistent electron and heavy-particle kinetics in a low pressure N_2 – O_2 glow discharge *Plasma Sources Sci. Technol.* **6** 373–85
- [45] Nahorny J, Ferreira C M, Gordiets B, Pagnon D, Touzeau M and Vialle M 1995 Experimental and theoretical investigation of a N_2 – O_2 DC flowing glow discharge *J. Phys. D: Appl. Phys.* **28** 738–47
- [46] Boisse-Laporte C, Chave-Normand C and Marec J 1997 A microwave plasma source of neutral nitrogen atoms *Plasma Sources Sci. Technol.* **6** 70–7
- [47] Ricard A, Moisan M and Moreau S 2001 Determination, through titration with NO, of the concentration of oxygen atoms in the flowing afterglow of Ar– O_2 and N_2 – O_2 plasmas used for sterilization purposes *J. Phys. D: Appl. Phys.* **34** 1203–12
- [48] Mrázková M, Vašina P, Kudrle V, Tálský A, Pintassilgo C D 2009 and Guerra V On the oxygen addition into nitrogen post-discharges *J. Phys. D: Appl. Phys.* **42** 075202
- [49] Gordiets B F, Ferreira C M, Guerra V L, Loureiro J M A H, Nahorny J, Pagnon D, Touzeau M and Vialle M 1995 Kinetic model of a low-pressure N_2 – O_2 flowing glow discharge *IEEE Trans. Plasma. Sci.* **23** 750–67
- [50] Gordiets B F and Ferreira C M 1998 Self-consistent modeling of volume and surface processes in air plasma *AIAA J.* **36** 1643–51
- [51] Hikida T and Mori Y 1978 Induced dissociation of $NO(B^2\Pi, v' = 9)$ by N_2 *J. Chem. Phys.* **69** 346–9
- [52] Pintassilgo C D, Loureiro J and Guerra V 2005 Modelling of a N_2 – O_2 flowing afterglow for plasma sterilization *J. Phys. D: Appl. Phys.* **38** 417
- [53] Bose D and Candler G 1996 Thermal rate constants of the $N_2+O\rightarrow NO+N$ reaction using ab initio $^3A''$ and $^3A'$ potential energy surfaces *J. Chem. Phys.* **104** 2825–33
- [54] Adamovich I V, Macheret S O, Rich J W and Treanor C E 1995 Vibrational relaxation and dissociation behind shock waves: I. Kinetic rate models *AIAA J.* **33** 1064–9
- [55] Adamovich I V, Macheret S O, Rich J W and Treanor C E 1998 Vibrational energy transfer rates using a forced harmonic oscillator model *J. Thermophys. Heat Transfer.* **12** 57–65

- [56] Lino da Silva M, Guerra V and Loureiro J 2007 State-resolved dissociation rates for extremely nonequilibrium atmospheric entries *J. Thermophys. Heat Transfer* **21** 40–9
- [57] Lino da Silva M, Guerra V and Loureiro J 2009 A review of non-equilibrium dissociation rates and models for atmospheric entry studies *Plasma Sources Sci. Technol.* **18** 034023
- [58] Macheret S O, Rusanov V D, Fridman A A and Sholin G V 1978 Synthesis of nitrogen oxides in a nonequilibrium plasma *Sov. Tech. Phys. Lett.* **4** 140–2
- [59] Macheret S O, Rusanov V L, Fridman A A and Sholin G V 1980 Nonequilibrium plasmachemical synthesis of nitrogen oxides *Sov. Phys. Tech. Phys.* **25** 421–7
- [60] Sá P A and Loureiro J 1997 A time-dependent analysis of the nitrogen afterglow in N_2 and N_2 -Ar microwave discharges *J. Phys. D: Appl. Phys.* **30** 2320–30
- [61] Kim Y C and Boudart M 1991 Recombination of O, N, and H atoms in silica: kinetics and mechanism *Langmuir* **7** 2999–3005
- [62] Pintasilgo C D, Guerra V, Guaitella O and Rousseau A 2010 Modelling of an afterglow plasma in air produced by a pulsed discharge *Plasma Sources Sci. Technol.* **19** 055001 1–14
- [63] Macko P, Veis P and Cernogora G 2004 Study of oxygen atom recombination on a pyrex surface at different wall temperatures by means of time-resolved actinometry in a double pulse discharge technique *Plasma Sources Sci. Technol.* **13** 251–62
- [64] Kutasi K, Guerra V and Sá P 2010 Theoretical insight into Ar- O_2 surface-wave microwave discharges *J. Phys. D: Appl. Phys.* **43** 175201
- [65] Piper L G 1988 State-to-state $N_2(A^3\Sigma_u^+)$ energy-pooling reactions: I. The formation of $N_2(C^3\Pi_u)$ and the Herman infrared system *J. Chem. Phys.* **88** 231–9
- [66] Gat E, Gherardi N, Lemoing S, Massines F and Ricard A 1999 Quenching rates of $N_2(C, v')$ vibrational states in N_2 and He glow silent discharges *Chem. Phys. Lett.* **306** 263–8
- [67] Pancheshnyi S V, Starikovskaia S M and Starikovskii A Yu 2000 Collisional deactivation of $N_2(C^3\Pi_u, v = 0, 1, 2, 3)$ states by N_2 , O_2 , H_2 and H_2O molecules *Chem. Phys.* **262** 349–57